Research Article

Received: 18 March 2021 Revised: 22 April 2021 Accepted article published: 5 May 2021 Published online in Wiley Online Library: 24 May 2021

(wileyonlinelibrary.com) DOI 10.1002/pi.6254

Highly heat-resistant branched silicon-containing arylacetylene resins with low curing temperature

Zhipeng Ling, Junli Zhu, Chunhua Cai,* Jiaping Lin,* Liquan Wang and Lei Du

Abstract

Silicon-containing arylacetylene (PSA) resins exhibit excellent thermal stability. However, the high curing temperature limits their applications. Herein, we report that changing the topology of PSA resins from linear to branched effectively decreases their curing temperature with no deterioration of thermal stability. Two sets of resins based on silyleneethynylene–naphthalene–ethynylene (SNP) and silyleneethynylene–phenyl–ethynylene (SPN) repeat units were studied. It is found that the branched resins exhibit considerably lower thermal curing temperatures than their linear counterparts. The exothermic peaks for branched SNP (BSNP) and branched SPN (BSPN) are about 190 and 214 °C, respectively, which are 18 and 25 °C lower than those for their linear counterparts (i.e. PSNP and PSPN). Density functional theory was applied to theoretically explain the differences in the thermal curing temperature between the linear and branched resins. The lower curing temperature of the branched PSAs is attributed to the greater number of terminal alkyne groups per molecule which increases the reactivity of the curing reaction to transform into a crosslinked structure. In addition, T_{d5} (the temperature at 5% mass loss) for BSNP and BSPN resins are 653 and 613 °C, respectively, which are comparable with those for their linear counterparts.

Keywords: heat-resistant polymers; silicon-containing arylacetylene resins; branched topology; curing temperature; thermal stability; density functional theory

INTRODUCTION

Over the past few decades, heat-resistant polymers exhibiting excellent thermal stability have received considerable attention for their applications in the fields of aerospace, aviation, electronics and so forth.[1,2] The most widely studied thermally resistant polymers include polyimide, phthalonitrile and polyarylacetylene. The main drawbacks that are usually encountered with these polymers are the poor processing properties, such as high melting point, high curing temperature and high heat release.[3–7] By introducing silica into the backbone of polyarylacetylene, Itoh *et al.* prepared a new kind of polymer, i.e. silicon-containing polyarylacetylene (PSA), which exhibited relatively better heat resistance and processability than traditional polyarylacetylene resins.[8–10] Homrighausen and Keller,[11] Du and co-workers[12,13] and other groups[14–16] have pushed this research by designing diverse chemical structures of PSA resins. However, the thermal stability and processability of PSA resins still need to be improved further for applications in aerospace and aviation areas.

Traditional design of heat-resistant PSAs based on trial-and-error experiments is time-consuming and usually cannot well balance the thermal and processing properties. Theoretical simulations have emerged as a powerful tool for investigating the relations between structures and properties of polymers. Theoretical simulation methods such as density functional theory (DFT) and molecular dynamics (MD) can predict the performance of polymers and explain experimental results, which can accelerate the discovery and design of high-performance materials. Recently, our group has applied a material genome approach to design new heat-resistant PSA resins.[17,18] For example, a novel resin comprising genes of dichlorodimethylsilane and 2,7-diethynylnaphthalene was designed. The novel resin, named poly(dimethylsilyleneethynylene–naphthalene–ethynylene) (PSNP), displayed a significantly high thermal resistance (T_{d5} reaches 648 °C).[18]

Besides the heat-resistant property, the processing property of resins is another important factor that affects their application performance. However, the thermal curing temperature of PSA resins is usually higher than 200 °C, which limits their further applications.[19–23] In addition to designing new chemical structures, some efforts have been devoted to decreasing the curing temperature of PSAs.[24–27] For example, introducing catalysts can decrease the curing temperature of PSA resins.[25] However, the

* *Correspondence to: C Cai or J Lin, Shanghai Key Laboratory of Advanced Polymeric Materials, Key Laboratory for Ultrafine Materials of Ministry of Education, School of Materials Science and Engineering, East China University of Science and Technology, Shanghai 200237, China. E-mail: caichunhua@ecust.edu.cn (Cai); jlin@ecust.edu.cn (Lin)*

Shanghai Key Laboratory of Advanced Polymeric Materials, Key Laboratory for Ultrafine Materials of Ministry of Education, School of Materials Science and Engineering, East China University of Science and Technology, Shanghai, China

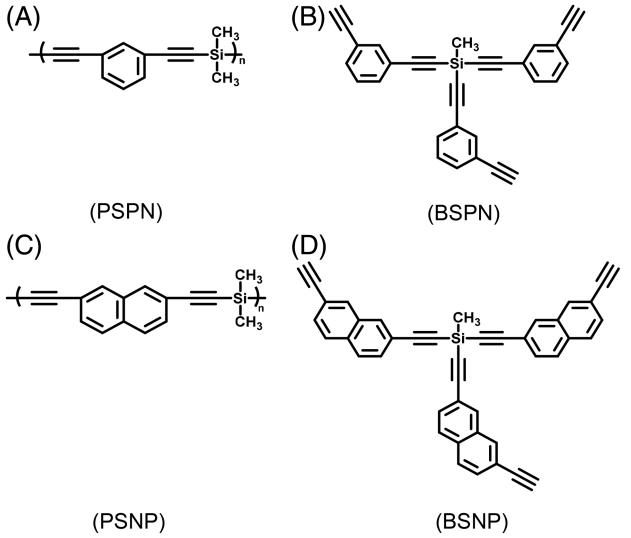

Scheme 1. Chemical structures of (a) PSPN, (b) BSPN, (c) PSNP and (d) BSNP resins.

remaining metal ions could affect the dielectric properties of the resulting polymers. In some cases, mixing with other polymers decreases the curing temperature of PSA resins.[26] However, this usually lowers the heat resistance of the resins. It is necessary to develop a new strategy to lower the curing temperature of PSA resins without affecting their thermal performance and other properties.

It is well known that the topology of polymers is also an important factor influencing their properties.[28–30] As compared with their linear counterparts, branched polymers have more reactive sites, which could increase their reactivity. Therefore, branched resins could be cured at a lower temperature. Furthermore, it can be deduced that less intermolecular entanglement could decrease the melt viscosity of polymers, which is advantageous for processing.[31,32]

In this paper, we report that changing the topology of PSA resins from linear to branched can effectively decrease their curing temperature while retaining their excellent thermal stability. A set of novel PSA resins, with both linear and branched topologies based on a novel silyleneethynylene–naphthalene–ethynylene (SNP) repeat unit, were synthesized. The linear resin, PSNP, has recently been reported,[18] and the branched resin, named branched methyltris(silyleneethynylene–naphthalene–ethynylene) (BSNP), is reported for the first time in this work. In addition, a set of traditional PSA resins based on silyleneethynylene–phenyl–ethynylene (SPN) repeat units with linear architecture named poly(dimethylsilyleneethynylene–phenyl–ethynylene) (PSPN) and with branched architecture named branched methyltris(silyleneethynylene–phenyl–ethynylene) (BSPN) were also synthesized and studied as references for evaluating the architecture–property relationship of the PSA resins. The structures of these four kinds of PSA resins, that is, BSPN, PSPN, BSNP and PSNP, are presented in Scheme 1. The effects of the topology of the resins on their properties, including thermal resistance, curing temperature and melt viscosity, were studied. We first synthesized the linear and branched resins using Grignard reagent reactions. Then the processing properties, including curing behavior and viscosity, were investigated experimentally. Theoretical calculations such as DFT and MD approaches were performed to further explain the experimental results including curing reactivity and melt viscosity of the resins. Finally, the thermal stability of the cured resins was also investigated.

EXPERIMENTAL

Materials

Triethylamine, methanol, potassium carbonate, tetrahydrofuran (THF), copper(I) iodide, tetrakis(triphenylphosphine)palladium, dichloromethane, *n*-hexane, methyl *tert*-butyl ether hydrochloric acid, 2,7-dibromonaphthalene and ethynyltrimethylsilane were purchased from Shanghai Titan Technology Co. Ltd. Methyltrichlorosilane, *m*-diethynylbenzene and ethylmagnesium bromide

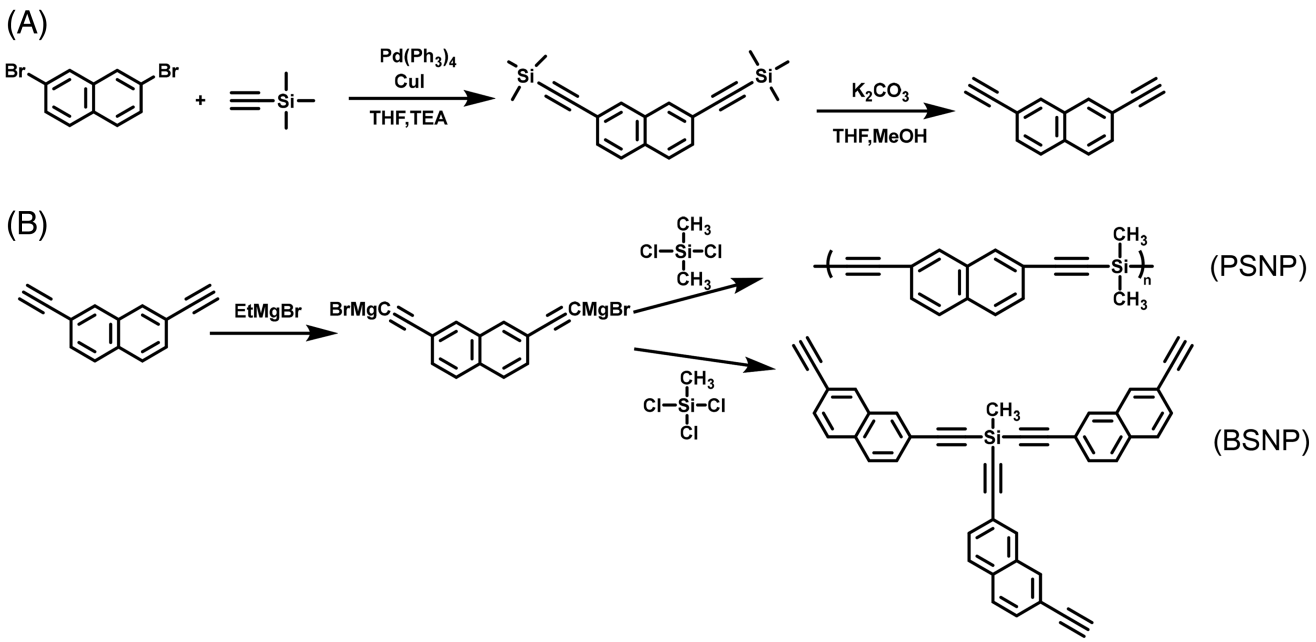

Scheme 2. Synthesis routes of (a) 2,7-diethynylnaphthalene and (b) PSNP and BSNP resins.

(1.0 mol L^{-1} solution in THF) were purchased from Aldrich Chemical. All reagents were used as received.

Synthesis of PSA resins

The PSA resins, namely PSPN, BSPN, PSNP and BSNP, were synthesized using Grignard reagent reactions from two kinds of essential regents,[33,34] i.e. diynes (2,7-diethynylnaphthalene for SNP resins and *m*-diethynylbenzene for SPN resins) and chlorosilanes (dichlorodimethylsilane for linear resins and methyltrichlorosilane for branched resins). For these essential regents, *m*-diethynylbenzene, dichlorodimethylsilane and methyltrichlorosilane are commercially available, while 2,7-diethynylnaphthalene was synthesized in our laboratory. The synthesis conditions for these resins were similar. We take BSNP, a novel PSA resin, as an example to describe the details of the synthesis procedures.

Synthesis of 2,7-diethynylnaphthalene

2,7-Diethynylnaphthalene was synthesized via a Sonogashira cross-coupling reaction (Scheme 2(a)).[35,36] (i) Synthesis of 2,7-bis((trimethylsilyl)ethynyl)naphthalene. In a 500 mL eggplant-shaped reaction flask, THF (100 mL) and trimethylamine (100 mL) were added under nitrogen into 2,7-dibromonaphthalene (10.02 g, 34.97 mmol), $Pd(Ph_3)_4$ (0.81 g, 0.71 mmol) and CuI (0.27 g, 1.42 mmol). The mixture was stirred vigorously at 50 °C for about 40 min, followed by the addition of ethynyltrimethylsilane (10.29 g, 0.24 mol) via a syringe. Then the solution was stirred at 50 °C for another 8 h under inert atmosphere, and the dark precipitate appeared that was removed by filtration after the reaction had finished. The filtrate was washed with deionized water three times, and the aqueous phase was extracted with ethyl acetate. The combined organic layer was concentrated under reduced pressure to remove the solvent. The residue was purified by silica gel column chromatography (*n*-hexane as eluent) to give 2,7-bis((trimethylsilyl)ethynyl)naphthalene in a yield of 91.61% (10.25 g) as a yellow solid. ^{1}H NMR (400 MHz, $CDCl_3$; δ, ppm): 7.91–7.52 (m, 6H, Ar-H), 0.29 (s, 18H, —CH_3). EI-MS (*m/z*): 320 [M^+]. Anal. Calcd for $C_{20}H_{24}Si_2$ (%): C, 75.00; H, 7.50. Found (%): C, 75.02; H, 7.33. (ii) Synthesis of 2,7-diethynylnaphthalene. Potassium carbonate (41.89 g, 0.31 mol) was added to a solution of 2,7-bis((trimethylsilyl)ethynyl)naphthalene (9.72 g, 30.32 mmol) in THF (50 mL) and methanol (50 mL). The solution was allowed to stir for 10 h at room temperature under nitrogen. Then the reaction mixture was washed with deionized water, and the aqueous phase was extracted with ethyl acetate. The combined organic layer was dried over magnesium sulfate and concentrated by rotary evaporation. The obtained crude powder was purified by silica gel column chromatography (*n*-hexane as eluent) to afford 2,7-diethynylnaphthalene in a yield of 95.34% (5.12 g) as pale yellow solid. ^{1}H NMR (400 MHz, $CDCl_3$; δ, ppm): 7.97–7.53 (m, 6H, Ar-H), 3.17 (s, 2H, C≡C—H). EI-MS (*m/z*): 176 [M^+]. Anal. Calcd for $C_{14}H_8$ (%): C, 95.45; H, 4.54. Found (%): C, 94.96; H, 4.64.

Synthesis of BSNP resin

The synthesis route of BSNP is shown in Scheme 2(b). A 250 mL four-necked flask was equipped with a condenser, a constant pressure dropping funnel, a thermometer and a nitrogen purge. The flask was then flame-dried under vacuum and back-filled with dry nitrogen three times. Ethylmagnesium bromide (12 mL, 12 mmol) was transferred into the reaction flask, which was immersed in an ice–water bath. To the solution, 2,7-diethynylnaphthalene (2.51 g, 14.26 mmol) in 30 mL of THF was added dropwise for 30 min. The reaction mixture was slowly heated to 68 °C and stirred for another 2 h, resulting in the formation of a gray suspension. The flask was then cooled with an ice–water bath, and a solution of methyltrichlorosilane (0.71 g, 4.73 mmol) in THF (20 mL) was added dropwise for about 15 min. After complete addition, the ice–water bath was removed, and the reaction was further refluxed for another 2 h. After cooling, 8% aqueous hydrochloric acid (50 mL) and methyl *tert*-butyl ether (100 mL) were added to the flask slowly. The resulting organic layer was separated out and washed with deionized water until the pH of the washed water was neutral. Then the orange solution was dried over anhydrous sodium sulfate. Finally, the resin was obtained after solvent removal by rotary evaporation and exposure to reduced pressure at 50 °C for 5 h. The resin was obtained in a yield of 93% (2.51 g) as a yellow solid. The PSPN and BSPN resins were cured according to the following procedure: 190 °C/2 h + 210 °C/2 h + 230 °C/2 h + 250 °C/2 h. The PSNP and BSNP resins were cured according to the following procedure: 160 °C/2 h + 180 °C/2 h + 200 °C/2 h + 230 °C/2 h.

Characterization

^{1}H NMR, ^{13}C NMR and ^{29}Si NMR spectra were obtained with a Bruker Avance 400 instrument using tetramethylsilane as an internal standard in $CDCl_3$. Fourier transform infrared (FTIR) spectra were acquired with a Nicolet iS50, the samples being prepared using the KBr pellet method. Mass spectra were recorded using a GCT Premier EI-TOF high-resolution time-of-flight mass spectrometer. DSC was performed with a TA Q2000 at heating rates of 5, 10, 15 and 20 °C min^{-1} under a nitrogen atmosphere from ambient temperature to 300 °C. Rheological behaviors were determined with a RheoStress RS600 rheometer at a heating rate of 2.0 °C min^{-1} and a shear rate of 0.01 s^{-1}. TGA was carried out with a TA Instruments SDT Q600 analyzer under nitrogen atmosphere at a heating rate of 10 °C min^{-1}. Pyrolysis–gas chromatography–mass spectrometry (Py-GC-MS) analyses were conducted with a Frontier Lab PY-2020i single-shot pyrolyzer and a Shimadzu GCMS-QP2010 chromatograph/mass spectrometer. Pyrolysis was carried out at 790 °C.

MD simulations

MD simulations were used to compute the viscosity (η) of resins as well as the mean squared displacement (MSD) of the resin molecules.[37] In the simulations, 80 resin molecules were placed in a simulation box under periodic boundary conditions, using the Amorphous Cell modulus. The initial density was set to be 0.5. Then geometry optimization was performed, and an equilibrium process with a total duration of 1 ns, under isobaric–isothermal (NPT) ensemble ($T = 800$ K, $P = 1$ atm), was used to obtain an equilibrium system. The system was then annealed to 400 K (cooling rate: 0.1 K ps^{-1}), multiple simulation processes for viscosity (under NPT ensemble) and MSD (under canonical (NVT) ensemble) data acquisition were performed for 1 ns. The shear viscosity was obtained by analyzing the trajectories of the simulations, and the MSD of the resin molecules was obtained directly from the particle positions in the simulations. The processes can be easily completed by the Analysis of Forcite modulus.

The procedure, including model construction, geometry optimization, MD simulations under NPT and NVT ensembles and analysis of shear viscosity and MSD, was realized with Materials Studio.[38] The Andersen thermostat and the Berendsen barostat were applied to control the temperature and pressure, respectively. The COMPASS force field was adopted

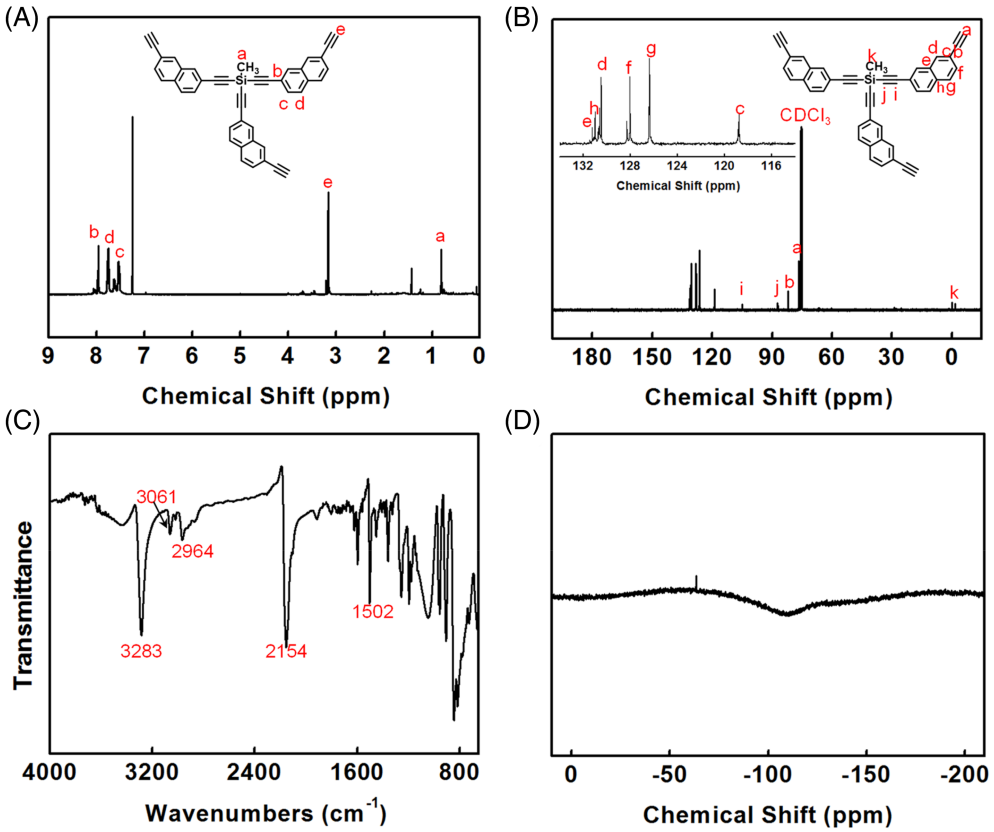

Figure 1. (a) ^{1}H NMR, (b) ^{13}C NMR, (c) FTIR and (d) ^{29}Si NMR spectra of BSNP resin.

throughout the simulations.[39] The Ewald summation method was used to sum the long-range electrostatic interaction terms, while the direct atom-based method was chosen for the short-range van der Waals interactions. The periodic boundary condition was considered to define the interaction of atoms in boundaries with the neighboring cells. The time step was set to 1.0 fs.

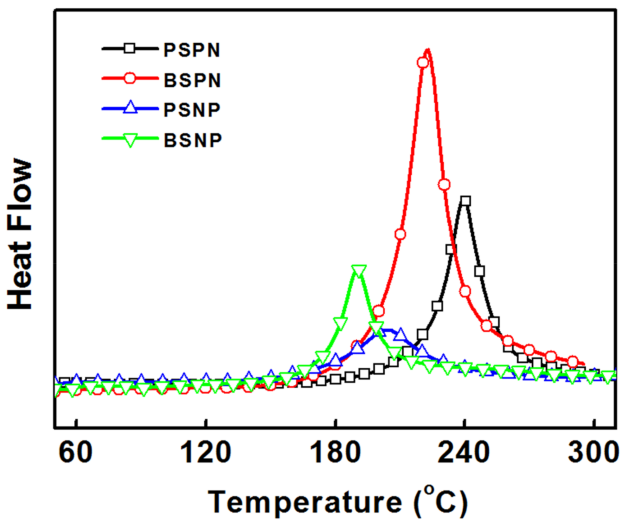

Figure 2. DSC curves of PSPN, BSPN, PSNP and BSNP resins at a heating rate of 10 °C min^{-1}.

RESULTS AND DISCUSSION

Structural characterization of BSNP resin

The chemical structure of the BSNP resin was characterized using ^{1}H NMR, ^{13}C NMR, FTIR and ^{29}Si NMR spectra (Fig. 1). Figure 1(a) shows the ^{1}H NMR spectrum of the BSNP resin. The three resonance peaks at 7.47, 7.59 and 7.70 ppm can be assigned to the phenyl protons. The peak at 3.09 ppm corresponds to ethynyl protons. The peak at 0.73 ppm corresponds to the chemical shift of methyl protons on silicon. Figure 1(b) shows the ^{13}C NMR spectrum of the BSNP resin. The peaks for inner acetylenic carbons appear at 87.2 and 105.0 ppm, respectively. The peaks at 76.6 and 82.0 ppm are assigned to the terminal acetylenic carbons. The chemical shifts of phenyl carbons are between 118.8 and 131.2 ppm. The peak at −1.50 ppm is attributed to the carbon connected to the silicon. The FTIR spectrum of BSNP is shown in Fig. 1(c). The band at 3283 cm^{-1} is due to the stretching vibration

Table 1. DSC results for PSPN, BSPN, PSNP and BSNP resins

Sample	Exothermic temperature (°C) T_i	T_p	T_f	Cure enthalpy (J g^{-1})
PSPN	214.5	239.2	256.4	443.9
BSPN	197.5	213.8	235.3	940.9
PSNP	185.2	207.6	230.1	232.8
BSNP	175.3	190.0	204.8	332.6

Heating rate: 10 °C min^{-1}.

Table 2. Peak temperatures and activation energies of PSPN, BSPN, PSNP and BSNP resins

Sample	Peak temperature (°C)				E_a (kJ mol^{-1})	
	5 °C min^{-1}	10 °C min^{-1}	15 °C min^{-1}	20 °C min^{-1}	Kissinger	Ozawa
PSPN	227.2	239.2	245.7	251.4	117.6	119.9
BSPN	203.0	213.8	222.3	226.7	106.9	109.6
PSNP	193.8	207.6	213.5	217.8	101.2	103.8
BSNP	177.4	190.0	195.4	201.0	96.2	99.3

of C—H in —C≡CH while the band corresponding to the stretching vibration of —C≡C— can be observed at 2154 cm^{-1}.The bands at 3061 and 1502 cm^{-1} correspond to C—H and C—C vibrations in the benzene ring, respectively. The band at 2964 cm^{-1} is assigned to the vibration of C—H in —CH_3 attached to the silicon atom. Figure 1(d) shows the ^{29}Si NMR spectrum of the BSNP resin. The peak observed at 63.34 ppm can be assigned to the silicon and the broad peak at −110 ppm may result from silicon dioxide in the NMR tube.

These characterizations suggest the successful synthesis of the BSNP resin. In addition, the other resins, PSNP, PSPN and BSPN, were also synthesized and investigated. In the following sections, the thermal curing behavior and melt viscosity of these PSA resins are discussed, together with the thermal stabilities of the cured resins, and the effect of the topology on the performance of the resins is analyzed.

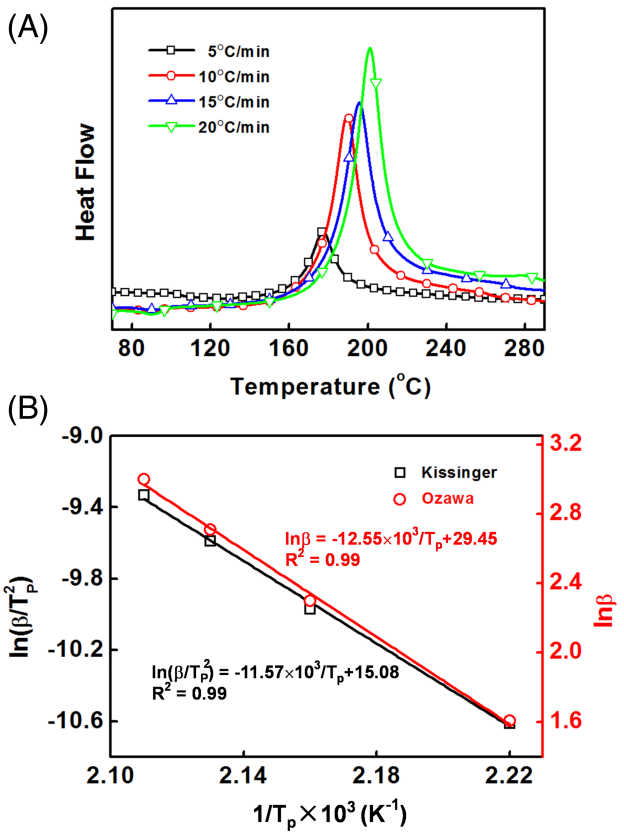

Figure 3. (a) DSC curves of BSNP resin at various heating rates. (b) Kissinger and Ozawa plots for determination of the activation energy of BSNP resin.

Thermal curing behaviors of the resins

The thermal curing behaviors of the PSA resins were characterized using DSC (Fig. 2), and the corresponding data are collected in Table 1. As can be seen, the initial curing temperatures (T_i) for PSPN, BSPN, PSNP and BSNP resins are 214.5, 197.5, 185.2 and 175.3 °C, respectively. The exothermic peak temperatures (T_p) for PSPN, BSPN, PSNP and BSNP resins are 239.2, 213.8, 207.6 and 190.0 °C, respectively. The cure enthalpies of PSPN, BSPN, PSNP and BSNP resins are 443.9, 940.9, 232.8 and 332.6 J g^{-1}, respectively. From these results, we can draw two conclusions. (i) The branched resins can be cured at a lower temperature but release more heat during the thermal curing process than their linear counterparts. The reasons are as follows. For branched resins, there are more terminal alkyne groups per molecule, which effectively augment the chance of valid collisions between reactive sites to form a crosslinked structure, therefore increasing the reactivity of the curing reaction (cured at a lower temperature). However, the existence of more reactive groups also inevitably leads to an increase in heat release of the branched resins. (ii) The SNP resins have lower curing temperature than the SPN resins. The higher π-donor effect of naphthalene groups than benzene groups can reduce the activation barrier of the dimerization which is the rate-determining step during the curing reaction, leading to a lower curing temperature of the SNP resins.[40–42]

The thermal curing properties of these resins were further characterized by the activation energy (E_a) of the curing reactions using classical Kissinger and Ozawa methods.[43,44] The relevant equations are as follows:

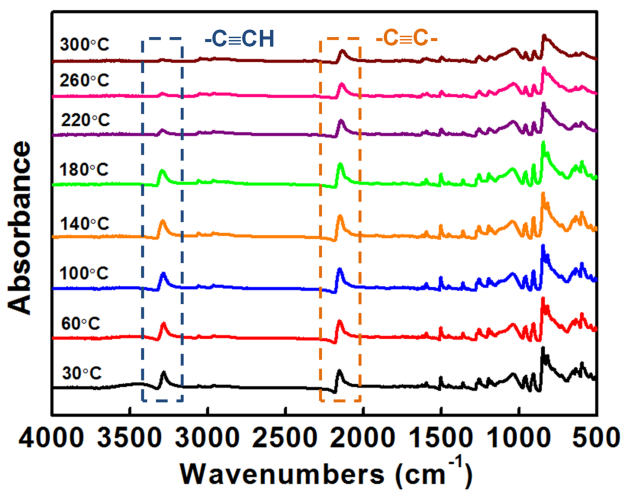

Figure 4. FTIR spectra of BSNP resin cured at different temperatures.

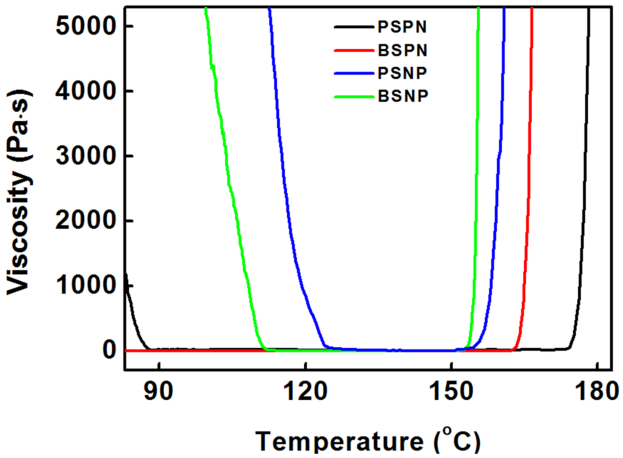

Figure 5. Viscosity–temperature curves of PSPN, BSPN, PSNP and BSNP resins.

$$\ln\frac{\beta}{T_p^2}=\ln\frac{AR}{E_a}-\frac{E_a}{RT_p} \quad (1)$$

$$\ln\beta=-\frac{1.0512E_a}{RT_p}+C \quad (2)$$

where β is the heating rate, T_p is the peak temperature, A is the preexponential factor, R is the gas constant, E_a is the activation energy and C is a constant. Figure 3(a) shows the DSC curves for the BSNP resin at various heating rates to obtain T_p. Then $\ln\beta/T_p^2$ *versus* $1/T_p$ and $\ln\beta$ *versus* $1/T_p$ are separately plotted and fitted (Fig. 3(b)). The activation energy of the BSNP resin can be calculated from the slope of the two lines.

Similarly, the curing kinetic parameters, including peak temperature at different heating rates and E_a value of the PSNP, PSPN and BSPN resins, were also obtained. These E_a values are listed in Table 2. As can been seen, the E_a values of the branched resins are smaller than those of their linear counterparts, and the SNP reins have smaller E_a values than the SPN resins. These results support well our assumption that branched resins have lower curing temperatures than their linear counterparts.

To get a theoretical explanation for the lower curing temperature of the branched resins, we used DFT to compute the |HOMO − LUMO| values of PSPN, BSPN, PSNP and BSNP resins.[45] The HOMO, highest occupied molecular orbital, is associated with the electron-donating ability of a molecular, whereas the LUMO, lowest unoccupied molecular orbital, is related to the ability to accept electrons. In a previous study, we found that the |HOMO − LUMO| value is positively correlated with the curing temperature, and therefore |HOMO − LUMO| can be used as a proxy for curing temperature.[18] Generally, a smaller value of |HOMO − LUMO| corresponds to a lower curing temperature. The |HOMO − LUMO| values were calculated with Gaussian 09 software at the B3LYP/6-311G(d,p) level.[46] It was found that the |HOMO − LUMO| values for PSNP, BSNP, PSPN and BSPN resins are 4.29, 4.01, 4.92 and 4.87 eV, respectively. The energy gaps of SNP resins are lower than those of SPN resins, and the branched resins have lower energy gaps than their linear counterparts. Thus the BSNP resin exhibits the lowest |HOMO − LUMO| value, and it can be cured at the lowest temperature. These results well explain the experimental observations.

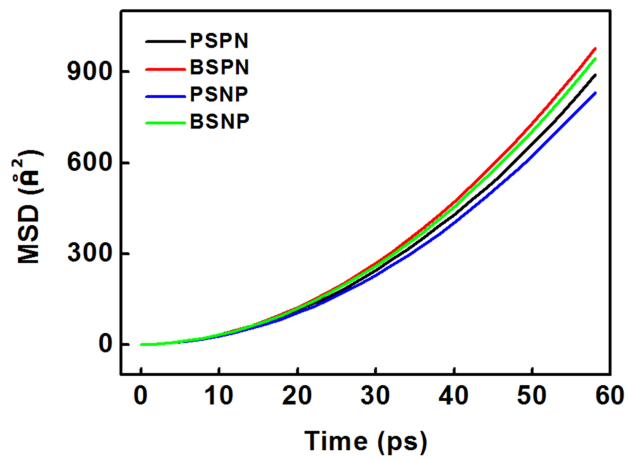

Figure 6. MSD curves of PSPN, BSPN, PSNP and BSNP resins.

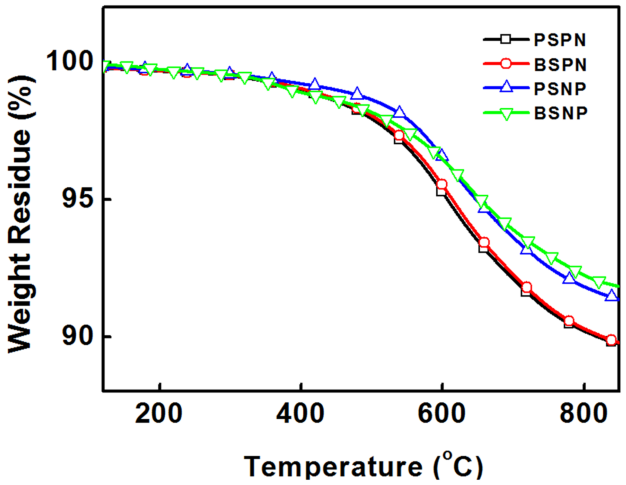

Figure 7. TGA curves of cured PSPN, BSPN, PSNP and BSNP resins (10 °C min^{-1} in nitrogen).

In addition to the curing temperature, the curing behavior of the BSNP resin was characterized using *in situ* FTIR spectroscopy by monitoring the changes of the functional groups in the thermosetting resin as a function of temperature (Fig. 4). The absorption peaks at 3284 and 2153 cm^{-1} were assigned to the stretching vibrations of the terminal alkyne hydrocarbon (—C≡C—H) and alkyne triple bond (—C≡C—), respectively. It was found that upon heating in the curing process, the intensity of the terminal alkyne (—C≡C—H) band reduced markedly and almost disappeared at 300 °C while the intensity of inner alkyne (—C≡C—) band

Table 3. TGA results for cured PSPN, BSPN, PSNP and BSNP resins

Sample	T_{d5} (°C)	$Y_{800°C}$ (%)
PSPN	606	90.1
BSPN	613	90.3
PSNP	648	91.8
BSNP	653	92.2

Heating rate: 10 °C min^{-1}, in nitrogen.

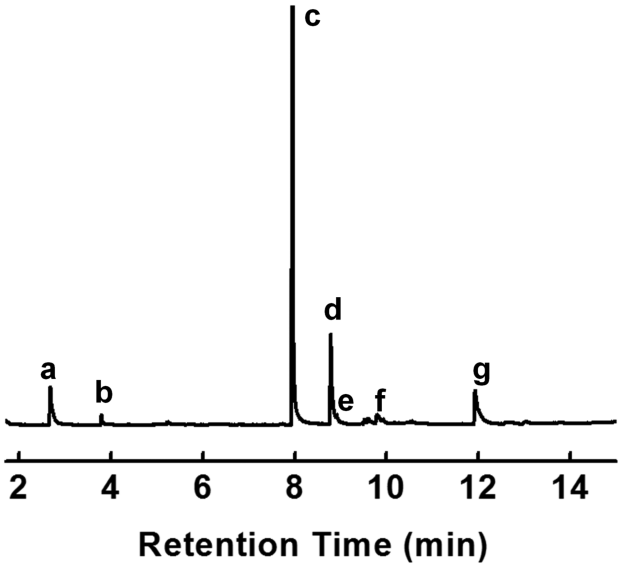

Figure 8. Py-GC-MS detection of gas products evolved from the pyrolysis of cured BSNP resin at 790 °C.

Table 4. Py-GC-MS analysis results of pyrolysis products of cured BSNP resin

Retention time (min)	M_w	Structure	Label[a]	Relative intensity (%)
2.70	78		a	5.04
3.81	91		b	1.26
7.96	128		c	71.03
8.79	142		d	12.26
8.92	156		e	3.24
9.60	178		f	0.63
11.93	204		g	6.53

Pyrolysis at 790 °C.
[a] Labels correspond to those in the Py-GC-MS spectrum displayed in Fig. 8.

weakened gradually and still can be observed at 300 °C. This implies that the reactivity of terminal alkyne (—C≡C—H) is higher than that of inner alkyne (—C≡C—). It is easier for branched resins that possess more terminal alkyne groups (—C≡C—H) in the molecules to participate in the curing reaction. In other words, the branched resins have lower curing temperatures than their linear counterparts, which is in accord with the results of DSC analysis. The specific crosslinked structures of BSNP at elevated temperature were analyzed using Py-GC-MS, as discussed in a later section.

Melt viscosity of resins

The viscosity of resins is essential to their processing properties. Figure 5 shows the variations of the viscosity of the PSPN, BSPN, PSNP and BSNP resins as a function of temperature. Due to the BSPN resin being gel-like at room temperature, its viscosity does not change significantly until 162 °C. And it increases sharply after 162 °C owing to the initiated thermal crosslinking reaction. Compared with BSPN, the softening point of PSPN, PSNP and BSNP reached about to 87, 131 and 112 °C, respectively. Though the gelation temperatures (at which viscosity increased rapidly) of PSNP and BSNP were not so very different (PSNP at 153 °C and BSNP at 151 °C), BSNP has a wider processing window than PSNP due to its decreased softening point, which is advantageous for processing such as resin transfer molding. Furthermore, apparent differences of the melt viscosity among the resins are observed.

On a quantitative level, the viscosity of PSNP (about 0.72 Pa s) was much higher than that of PSPN (about 0.52 Pa s), BSPN (about 0.21 Pa s) and BSNP (0.23 Pa s) at 140 °C. The branched resins (BSPN and BSNP) can effectively reduce chain entanglement between the molecules compared with PSPN and PSNP (linear) to lead to the melt resins flowing easily, but the higher molecular weight of BSNP makes its viscosity a little higher than that of BSPN. In a word, BSNP possesses a relatively wide processing window accompanied with low melt viscosity.

We then used equilibrium MD methods and the Green–Kubo formula to compute the viscosity (η) of the resins. The equilibrium MD methods, using the fluctuations of the stress tensor, can accurately estimate shear viscosity.[37] The computation reveals that the viscosity of the resins is closely related to the molecular structure. The viscosity values computed using MD for the PSNP, BSNP, PSPN and BSPN resins are 0.022, 0.014, 0.016 and 0.013 Pa s, respectively. These results indicate that the viscosity of the branched resins is lower than that of their linear counterparts. The difference in the viscosity of the branched and linear resins can be explained by the different MSD of the resin molecules.[47] A larger value of MSD denotes a stronger motion ability of the resin molecules; thus, a resin with larger MSD has a lower melt viscosity. The variations of the MSD curves for the resins are depicted in Fig. 6. It can be seen that the MSD values of the branched resins (BSPN and BSNP) are both larger than those of their linear counterparts, which results in a lower melt viscosity of the branched resins. The theoretical calculations are well consistent with the experimental results, and explain the origin of the lower melt viscosity of the branched resins.

Thermal stabilities and curing behavior of the resins

The thermal stability of the crosslinked resins was investigated using the TGA technique under nitrogen at a heating rate of 10 °C min^{-1} up to 850 °C. Figure 7 shows the TGA curves, and Table 3 lists the degradation temperature of 5% weight loss (T_{d5}) and the chair yield at 800 °C. As shown in Fig. 7, the cured PSPN and BSPN resins offered excellent thermal stability under nitrogen and gave chair yields of 90.1% and 90.3% when heated to 800 °C, and T_{d5} reached 606 and 613 °C, respectively. PSNP and BSNP exhibited better thermal stability with T_{d5} up to 648 and 653 °C, and chair yield up to 91.8% and 92.2%, respectively. This phenomenon is related to the greater number of naphthalene rings in the uncured PSNP and BSNP providing a large number of rigid groups in the cured molecules that require more energy to pyrolyze. Furthermore, more terminal alkyne groups in BSNP take part in the thermal curing reaction to increase crosslinking density, which makes BSNP the most heat-resistant resin among those investigated. Meanwhile, according to previous

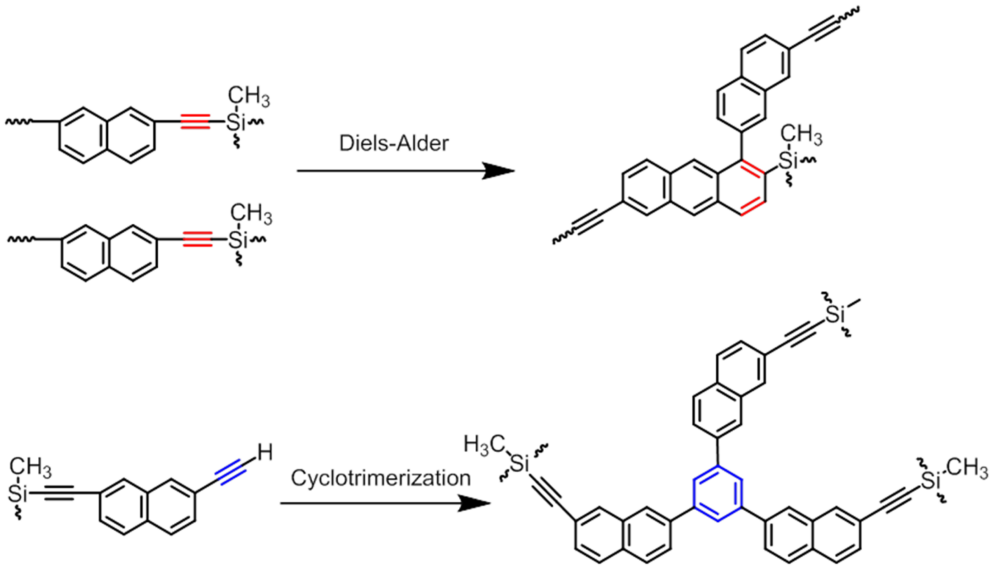

Scheme 3. Diels–Alder and cyclotrimerization reactions of BSNP upon curing. Red triple bond refers to inner alkyne groups and blue triple bond refers to terminal alkyne groups.

literature,[22] there would be other rigid aromatic rings in addition to naphthalene rings in the cured resin. In this regard, the cured BSNP resin was examined using Py-GC-MS analysis as discussed in the following.

Py-GC-MS is a useful tool for analyzing the structure of the cured BSNP resin. Figure 8 shows the total ion chromatogram (TIC) of the crosslinked BSNP obtained at 790 °C and the pyrolysis products are summarized in Table 4. As evident from Table 4, there are several fragments during pyrolysis, and the identified products can be divided into three groups: (i) phenyl ring volatiles and their derivatives, (ii) naphthyl ring volatiles and their derivatives and (iii) anthracene ring derivatives.

As compared with the original chemical structure of the resin, there appear two kinds of new fragments, that is, anthracene ring derivatives (peak f in Fig. 8) and naphthyl ring derivatives (peak g in Fig. 8). These new fragments could be formed through Diels–Alder and cyclotrimerization reactions of the C≡C group in the curing reaction.[48] These two reactions are presented in Scheme 3. Furthermore, the relative content of naphthyl ring derivatives (peak g) in pyrolysis products is much higher than that of anthracene ring derivatives (peak f), which suggests that the cyclotrimerization reaction takes the lead during curing reaction. Based on the Py-GC-MS and *in situ* FTIR analysis, the thermal curing process of the BSNP resin can be clearly revealed.

CONCLUSIONS

This study presented a new strategy in that changing the topology of PSA resins from linear to branched can decrease the curing temperature by retaining their thermal stability. Based on a novel chemical structural unit, i.e. SNP, both branched (BSNP) and linear (PSNP) resins were successfully prepared by Grignard reagent reactions. The exothermic peak temperature of the BSNP resin (about 190 °C) is 18 °C lower than that of its linear counterpart (PSNP), which is related to the increased number of reactive terminal alkyne groups of the branched resin. And the melt viscosity of the BSNP resin is about 0.23 Pa s, which could facilitate its applications. Theoretical simulations were applied to further explore the structure–property relations of the linear and branched resins. The lower curing temperature of the branched resins is explained by their lower |HOMO − LUMO| value, which corresponds to a higher curing reactivity. And the lower melt viscosity of the branched resins originates from the larger MSD, which increases the motion ability of the molecules. The thermal stability studies revealed that both the BSNP and PSNP resins have excellent thermal stability with T_{d5} of about 650 °C and residual yield at 800 °C under nitrogen of about 92%. The high heat resistance resulted from the crosslinked molecular structure initiated by Diels–Alder and cyclotrimerization reactions, the cyclotrimerization reaction dominating the curing reaction. Furthermore, the concept that decreasing the curing temperature of PSA resins by changing their topology from linear structure to branched structure is also verified by another set of PSA resins with both branched and linear topologies. This work emphasizes the effect of topology of the resins on their properties, and the information obtained could guide the design of novel heat-resistant resins.

ACKNOWLEDGEMENTS

This work was supported by the National Natural Science Foundation of China (52073095, 51833003 and 21975073).

REFERENCES

1 Houser EJ and Keller TM, *Macromolecules* **31**:4038 (1998).
2 Li J, Liang J, Jian X, Hu W, Li J and Pei Q, *Macromol Mater Eng* **299**:1403 (2014).
3 Liaw D-J, Wang K-L, Huang Y-C, Lee K-R, Lai J-Y and Ha C-S, *Prog Polym Sci* **37**:907 (2012).
4 Zong L, Liu C, Zhang S, Wang J and Jian X, *Polymer* **77**:177 (2015).
5 Wang M and Zhao T, *J Appl Polym Sci* **105**:2939 (2007).
6 Oishi SS, Botelho EC, Luscombe CK and Rezende MC, *Polímeros* **24**:541 (2014).
7 Wang M and Ning Y, *ACS Appl Mater Interfaces* **10**:11933 (2018).
8 Itoh M, Mitsuzuka M, Iwata K and Inoue K, *Macromolecules* **27**:7917 (1994).
9 Itoh M, Inoue K, Iwata K, Ishikawa J and Takenaka Y, *Adv Mater* **9**:1187 (1997).

10 Itoh M, Inoue K, Iwata K, Mitsuzuka M and Kakigano T, *Macromolecules* **30**:694 (1997).
11 Homrighausen CL and Keller TM, *J Polym Sci A Polym Chem* **40**:88 (2002).
12 Li F, Wang C, Shen X, Huang F and Du L, *Polym J* **43**:594 (2011).
13 Gao F, Zhang L, Tang L, Zhang J, Zhou Y, Huang F *et al*., *Bull Korean Chem Soc* **31**:976 (2010).
14 Liu HQ and Harrod JF, *Can J Chem* **68**:1100 (1990).
15 Ichitani M, Yonezawa K, Okada K and Sugimoto T, *Polym J* **31**:908 (1999).
16 Kimura H, Okita K, Ichitani M, Sugimoto T, Kuroki S and Ando I, *Chem Mater* **15**:355 (2003).
17 Zhou E, Wang L, Lin J, Zhu J, Du L, Deng S *et al*., *Acta Polym Sin* **50**:1322 (2019).
18 Zhu J, Chu M, Chen Z, Wang L, Lin J and Du L, *Chem Mater* **32**:4527 (2020).
19 Zhou Y, Huang F, Du L and Liang G, *Polym Eng Sci* **55**:316 (2015).
20 Bu X, Zhou Y and Huang F, *Mater Lett* **174**:21 (2016).
21 Zhou Q, Feng X, Ni L and Chen J, *J Appl Polym Sci* **102**:2488 (2006).
22 Chen M, Liu C and Lin J, *Polym Degrad Stab* **112**:35 (2015).
23 Chen H, Xin H, Lu J, Tang J, Yuan Q and Huang F, *High Perform Polym* **29**:595 (2016).
24 Gao Y, Zhou Y, Huang F and Du L, *High Perform Polym* **25**:445 (2013).
25 Shen Y, Yuan Q, Huang F and Du L, *Thermochim Acta* **590**:66 (2014).
26 Han M, Guo K, Wang F, Zhu Y and Qi H, *J Appl Polym Sci* **134**:45141 (2017).
27 Tseng W-C, Chen Y and Chang G-W, *Polym Degrad Stab* **94**:2149 (2009).
28 Cai C, Zhu W, Chen T, Lin J and Tian X, *J Polym Sci A Polym Chem* **47**: 5967 (2009).
29 Chen L, Chen T, Fang W, Wen Y, Lin S, Lin J *et al*., *Biomacromolecules* **14**: 4320 (2013).
30 Huang Y, Deng S and Liu Z, *J Appl Polym Sci* **136**:48248 (2019).
31 Kolel-Veetil MK, Dominguez DD, Klug CA and Keller TM, *Macromolecules* **42**:3992 (2009).
32 Yang M, Shi S, Wang M, Wang Y, Luo Z, Feng Z *et al*., *J Appl Polym Sci* **117**:714 (2010).
33 Li C, Luo J, Ma M, Tang J, Yuan Q and Huang F, *J Polym Sci A Polym Chem* **57**:2324 (2019).
34 Cai M, Yuan Q and Huang F, *Polym Int* **67**:1563 (2018).
35 Hachiya S, Asai K and Konishi G-i, *Tetrahedron Lett* **54**:1839 (2013).
36 Liu L, Liu Z, Xu W, Xu H, Zhang D and Zhu D, *Tetrahedron* **61**:3813 (2005).
37 Xu P, Lin J and Zhang L, *J Phys Chem C* **121**:28194 (2017).
38 BIOVIA Materials Studio. Available: https://www.3dsbiovia.com/products/collaborative-science/biovia-materials-studio/ [].
39 Sun H, *J Phys Chem B* **102**:7338 (1998).
40 Gandon S, Mison P, Bartholin M, Mercier R, Sillion B, Geneve E *et al*., *Polymer* **38**:1439 (1997).
41 Wessig P and Müller G, *Chem Rev* **108**:2051 (2008).
42 Fabig S, Janiszewski A, Floss M, Kreuzahler M and Haberhauer G, *J Org Chem* **83**:7878 (2018).
43 Kissinger HE, *Anal Chem* **29**:1702 (1957).
44 Ozawa T, *Thermochim Acta* **100**:109 (1986).
45 Mannodi-Kanakkithodi A, Chandrasekaran A, Kim C, Huan TD, Pilania G, Botu V *et al*., *Mater Today* **21**:785 (2018).
46 Frisch MJ, Trucks GW, Schlegel HB, Scuseria GE, Robb MA, Cheeseman JR *et al*., *Gaussian 09, Revision A.02*. Gaussian, Wallingford, CT (2009).
47 Yang Q, Li X, Shi L, Yang X and Sui G, *Polymer* **54**:6447 (2013).
48 Guo K, Li P, Zhu Y, Wang F and Qi H, *Polym Degrad Stab* **131**:98 (2016).

